



ORIGINAL ARTICLE

Facile synthesis of ZnO and Co₃O₄ nanoparticles by thermal decomposition of novel Schiff base complexes: Studying biological and catalytic properties



Asma S. Al-Wasidi^{a,*}, Ibtisam I.S. AlZahrani^a, Hotoun I. Thawibaraka^a,
Ahmed M. Naglah^{b,c}

^a Department of Chemistry, College of Science, Princess Nourah Bint Abdulrahman University, Riyadh 11671, Saudi Arabia

^b Department of Pharmaceutical Chemistry, Drug Exploration & Development Chair (DEDC), College of Pharmacy, King Saud University, Riyadh 11451, Saudi Arabia

^c Peptide Chemistry Department, Chemical Industries Research Division, National Research Centre, 12622 Dokki, Cairo, Egypt

Received 3 October 2021; accepted 5 December 2021

Available online 10 December 2021

KEYWORDS

Schiff base complexes;
Nanoparticles;
Photocatalytic degradation;
Methylene blue dye;
Biological activity

Abstract In this paper, a novel Zn(II) and Co(II) Schiff base complexes were synthesized by template method via refluxing 2,3-Naphthalenedicarboxaldehyde, Metal(II) chloride (Metal = Zn or Co), and L-phenylalanine. ZnO and Co₃O₄ nanoparticles were synthesized by thermal decomposition of Zn(II) and Co(II) complexes, respectively. The products were characterized using different instruments such as CHN, Conductivity, FT-IR, XRD, HR-TEM, and UV-Vis spectrophotometer. The experimental results of elemental analysis for Zn(II) and Co(II) complexes, agree with the calculated results, indicating that the Zn(II) and Co(II) complexes have 1:1 ligand/metal ratios. The molar conductance of the Zn(II) and Co(II) complexes, is less than 5 Ω⁻¹cm⁻¹mol⁻¹, confirming the non-electrolytic nature of the synthesized complexes. The average crystallite diameter of the ZnO and Co₃O₄ samples is 39.64 and 30.38 nm, respectively. The optical energy gap of the ZnO and Co₃O₄ samples are 2.75 and 3.25 eV, respectively. Methylene blue dye was utilized to examine the photocatalytic properties of the synthesized nanoparticles using UV irradiations in the absence and presence of hydrogen peroxide. The % degradation of the methylene blue dye in the presence of hydrogen peroxide using ZnO and Co₃O₄ samples after 40 min is 94.55 and 98.98, respectively. Six pathogenic microbes were utilized to examine the antimicrobial properties of the synthesized Schiff base complexes and their nanoparticles: Staphylococcus aureus, Escherichia coli, Pseudomonas

* Corresponding author.

E-mail address: asalwasidi@pnu.edu.sa (A.S. Al-Wasidi).

Peer review under responsibility of King Saud University.



Production and hosting by Elsevier

aeruginosa, Streptococcus species, Aspergillus species, and Candida species. Zn(II) and Co(II) complexes display inhibition towards all the studied microbes. Besides, ZnO and Co₃O₄ nanoparticles exhibit less inhibition towards Staphylococcus aureus, Escherichia coli, Pseudomonas aeruginosa, and Streptococcus species. Moreover, ZnO and Co₃O₄ nanoparticles have no activity towards Aspergillus and Candida species.

© 2021 The Author(s). Published by Elsevier B.V. on behalf of King Saud University. This is an open access article under the CC BY-NC-ND license (<http://creativecommons.org/licenses/by-nc-nd/4.0/>).

1. Introduction

Metal complexes of Schiff base are a field of increasing importance. These metal complexes were used for various applications such as treatment of cancer, antivirus agents, fungicide agents, and antibactericidal agents (Kaczmarek et al., 2018; Liang et al., 2021; Al-Resayes et al., 2016; Alaghaz et al., 2015). Also, metal complexes of Schiff base, which were gotten from amino acids, are discovering applications in understanding several in vivo biochemical reactions (Saikumari, 2021; Otani et al., 2021). Besides, the poisoning task of specific metal ions in living organisms is determined by exploiting these complexes via verifying the activity of the drug. Donmez et al. prepared a novel biosensor that is sensitive to glucose using the microspheres modified with (4-formyl-3-methoxyphenoxymethyl)polystyrene (FMPS) with l-glycine. Polymeric microspheres having Schiff bases were prepared from FMPS using the glycine condensation method. Glucose oxidase enzyme was immobilized onto modified carbon paste electrode by cross-linking with glutaraldehyde. Oxidation of enzymatically produced H₂O₂ (+0.5 V vs. Ag/AgCl) was used for determination of glucose. Optimal temperature and pH were found as 50 °C and 8.0, respectively. The glucose biosensor showed a linear working range from 5.0×10^{-4} to 1.0×10^{-2} M, $R^2 = 0.999$. Storage and operational stability of the biosensor were also investigated. The biosensor gave perfect reproducible results after 20 measurements with 3.3% relative standard deviation. It also had good storage stability (Donmez et al., 2017). Amino acids form the basic structural units of proteins and are chemical kinds required for performing an enormous number of biological purposes, as illustrated via the task of enzymes. Ortho-phthalaldehyde acts the main role in the assay of amino acids. The residues of amino acids in several biological fluids and enzymes are determined by exploiting ortho-phthalaldehyde. It achieves requests in the clinical area as a high-level antiseptic (Moitessier et al., 2020; Gyimesi-Forrás et al., 2005). Recently, great interest has been established in copper Schiff base complexes as fundamental models for the active position of the copper proteins. In the copper proteins, a distorted environment of mixed donor groups and low symmetry is present (Dinesh Karthik et al., 2020; Srivastava et al., 2021). Also, nickel complexes are existing in the active positions of urease (Thalamuthu and Neelakantan, 2021; Dong et al., 2012). In the presence of oxidizing agents, square planar nickel-salen was used in the cleavage of plasmid DNA as reported by Morrow and Kolasa (Morrow and Kolasa, 1992). Zinc-including bridged-carboxylate complexes have differed structural styles in hydrolytic metalloenzymes, for example, aminopeptidases and phosphatases (Baltulionis et al., 2021; Karmakar and Chattopadhyay, 2020). Latif et al synthesize a Schiff base via the condensation of 4-(dimethylamino)benzaldehyde and S-benzylthiocarbamate. Also, Ni(II), Cu(II), and Zn(II) complexes were synthesized. The results of the biological activity of the tested compounds displayed that the complexes were more effective antibiotics than the free Schiff base. The Ni(II) and Cu(II) complexes exhibited high antibacterial effectiveness whereas Zn(II) complex was moderately active against bacteria (Latif et al., 2019). Recently, the complexes have been exploited in the facile and low-cost synthesis of many nanomaterials of small crystallite size by thermal decomposition. Abdelghany et al synthesize Ag and CuO nanoparticles via thermal

decomposition of Ag(I) and Cu(II) Schiff base complexes, respectively. The Schiff base was synthesized by the condensation reaction between 2-hydroxy-1-naphthaldehyde and 3-methyl-4-amino-5-mercapto-1,2,4-triazole (Abdelghany et al., 2021). Katouah synthesizes ZnO and Co₃O₄ nanoparticles by thermal decomposition of Zn(II) and Co(II) Schiff base complexes, respectively. The Schiff base was synthesized via condensation of 4-(dimethylamino)benzaldehyde with 4-amino-5-ethyl-4H-1,2,4-triazole-3-thiol (Katouah, 2021). Nanomaterials are used in many applications, most notably the treatment of water pollutants by adsorption and photocatalytic degradation techniques (Abdelrahman, 2018; Hegazey et al., 2020; Abdelrahman and Hegazey, 2019; Abdelrahman et al., 2021). The photocatalytic degradation method is an effective and simple way to get rid of many dyes because it depends on the use of light and a catalyst to produce free radicals that can degrade these pollutants (Abdelrahman and Hegazey, 2019; Nguyen et al., 2021b; Nasri et al., 2021; Nguyen et al., 2021a; Nguyen et al., 2021c; Shokouhimehr et al., 2019; Nguyen et al., 2020; Kiani et al., 2020; Nayebi et al., 2020; Zhang et al., 2019). So, in this paper, Zn(II) and Co(II) complexes were synthesized by template method via refluxing 2,3-Naphthalenedicarboxaldehyde, cobalt(II) chloride hexahydrate or zinc(II) chloride, and L-phenylalanine. ZnO and Co₃O₄ nanoparticles were synthesized by thermal decomposition of the Zn(II) and Co(II) complexes, respectively. The biological and catalytic properties were studied.

2. Experimental

2.1. Chemicals

Methylene blue dye (C₁₆H₁₈ClN₃S), cobalt(II) chloride hexahydrate (CoCl₂·6H₂O), zinc(II) chloride (ZnCl₂), and L-phenylalanine (C₉H₁₁NO₂), ethanol (C₂H₅OH), sodium hydroxide (NaOH), and 2,3-Naphthalenedicarboxaldehyde (C₁₂H₈O₂) were of analytical grade (Purity = 99.99 %) and obtained from Sigma Aldrich Company and utilized without further purification.

2.2. Synthesis of Zn(II) and Co(II) Schiff base complexes

The template method is operated for the synthesis of Zn(II) and Co(II) Schiff base complexes. About 6 mmol (1.11 g) of 2,3-Naphthalenedicarboxaldehyde in 25 mL ethanol was added to an ethanolic solution of proper cobalt(II) chloride hexahydrate or zinc(II) chloride (6 mmol/25 mL) and stirred at room temperature for one hour. To this stirred solution, 12 mmol of L-phenylalanine in 25 mL of ethanol including 12 mmol sodium hydroxide was added then refluxed for six hours. After that, obtained solid product was filtered using filter paper, washed various times using ether, and then recrystallized from ethanol.

2.3. Synthesis of ZnO and Co₃O₄ nanoparticles

The Zn(II) and Co(II) Schiff base complexes were thermally decomposed at 550 °C for 5 h to produce ZnO and Co₃O₄ nanoparticles, respectively.

2.4. Characterization

Elemental analysis of Co(II) and Zn(II) Schiff base complexes was gotten using an Elementar elemental analyzer (Vario EL III). The molar conductance of the Co(II) and Zn(II) complexes in ethanol was assessed utilizing a conductivity bridge (Systronics 304). The Fourier transform (FT-IR) spectra of the complexes, ZnO, and Co₃O₄ samples, on KBr pellets, were gotten at room temperature using a Shimadzu spectrometer (IRTracer 100) in the range from 4000 to 400 cm⁻¹. Thermal analysis of the Co(II) and Zn(II) complexes was performed using TG/DTG instrument (Perkin-Elmer Diamond) through an oxygen atmosphere at a heating rate of 10 °C/min. The X-ray diffraction (XRD) patterns of the ZnO and Co₃O₄ samples were conducted utilizing a Bruker diffractometer (D8 Advance) with Cu-K α irradiation ($\lambda = 0.15$ nm) at 40 mA and 40 kV. The high-resolution transmission electron microscopy (HR-TEM) images of the ZnO and Co₃O₄ samples were taken using JEOL model 2100. Optical energy gaps of ZnO and Co₃O₄ samples were obtained using a UV-Vis spectrophotometer (Cintra 101).

2.5. Photocatalytic degradation of methylene blue dye

Degradation experiments of the methylene blue dye were achieved in a photochemical batch reactor containing a magnetic stirrer. 15 W four UV lamps ($\lambda = 365$ nm) were operated as a UV radiation source. All the experiments of adsorption and photocatalytic degradation started with a 60 mL aqueous solution of 60 mg/L of methylene blue dye and 0.15 g of ZnO or Co₃O₄. The adsorption experiments were achieved in the dark. The degradation of methylene blue dye in the absence and presence of hydrogen peroxide under the effect of UV light and catalyst (ZnO or Co₃O₄) was observed using a UV-Vis spectrophotometer at different periods. The concentration of methylene blue dye was determined from a preset calibration curve at 663 nm (maximum absorption wavelength of the methylene blue dye).

% Adsorption (% A) was calculated using Eq. (1) whereas % degradation (% D) was calculated using Eq. (2).

$$\%A = \left[\frac{Z_1 - Z_2}{Z_1} \right] \times 100 \quad (1)$$

$$\%D = \left[\frac{Z_2 - Z_3}{Z_2} \right] \times 100 \quad (2)$$

where Z_1 (mg/L) is the initial concentration of methylene blue dye, Z_2 (mg/L) is the concentration of methylene blue dye after adsorption in the dark place, and Z_3 (mg/L) is the concentration of methylene blue dye after exposure to UV light.

2.6. Biological activity

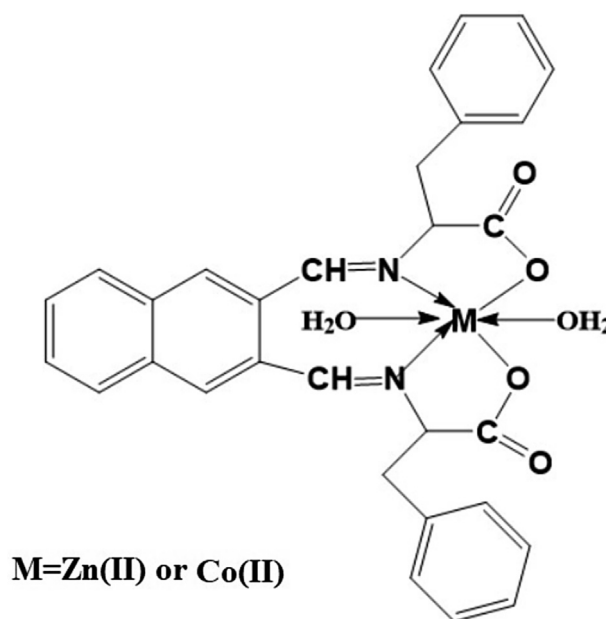
Six pathogenic microbes were utilized to examine the antimicrobial activity of the synthesized Schiff base complexes and

their nanoparticles: Staphylococcus aureus, Escherichia coli, Pseudomonas aeruginosa, Streptococcus species, Aspergillus species, and Candida species. The antimicrobial activity of the extracts was qualitatively estimated via a modified disc diffusion approach (Almehizia et al., 2021). A lawn of microorganisms was synthesized via pipetting and equally spreading inoculums (10^{-4} cm³, adjusted turbidometrically to 10^{-5} cfu cm³) onto agar group in petri dishes, utilizing potato dextrose agar in the case of fungi and Muller Hinton nutrient agar in the case of bacteria. The liquid media including the bacterial divisions was autoclaved for twenty minutes at 15 lb pressure and 120 °C before inoculation. Then, the bacteria were cultured at 37 °C in an incubator for one day. The samples (50 μ g) to be examined were dissolved in dimethyl sulfoxide then dropwise added to a Whatman No. 1 filter paper disc (10 mm diameter) placed at the center of each agar plate. These filter paper discs were then kept at 5 °C for one hour then transported to an incubator maintained at 37 °C. After four days, the inhibition zone, which formed around the discs in each plate, was determined. Commercially available nystatin was utilized as antifungal control whereas ampicillin was utilized for antibacterial control.

3. Results and discussion

3.1. Characterization of Zn(II) and Co(II) complexes

The experimental results of elemental analysis for the Zn(II) and Co(II) complexes agree with the calculated results indicating that the Zn(II) and Co(II) complexes have 1:1 ligand/metal ratios as clarified in Scheme 1 and Table 1. The molar conductance of the Zn(II) and Co(II) complexes in ~ 0.001 M ethanol at room temperature is 3.87 and 4.12 $\Omega^{-1}\text{cm}^{-1}\text{mol}^{-1}$, respectively. These values confirming the non-electrolytic nature of the synthesized complexes because of the absence of counterions in the suggested structure of the complexes as shown in



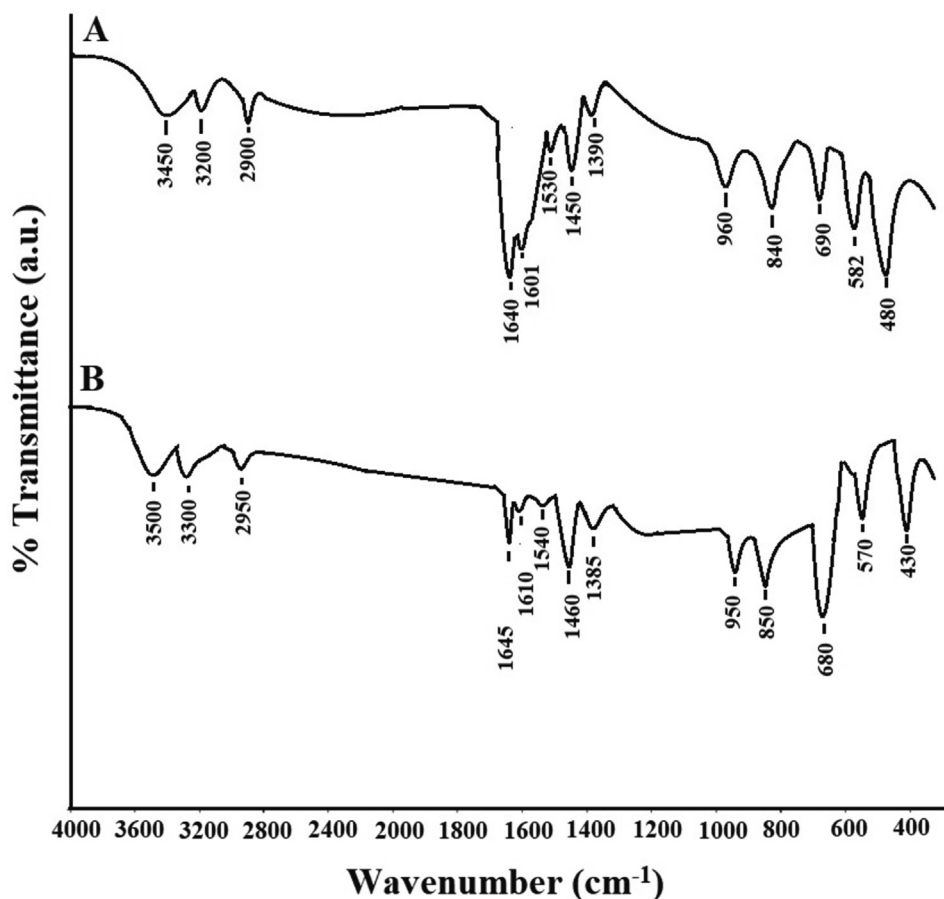
Scheme 1 The Structure of the synthesized complexes.

Table 1 Elemental analysis of the synthesized complexes.

% Element	Zn(II) complex Formula: C ₃₀ H ₂₈ N ₂ O ₆ Zn Molecular weight: 576.12		Co(II) complex Formula: C ₃₀ H ₂₈ N ₂ O ₆ Co Molecular weight: 571.13	
	Calculated	Found	Calculated	Found
%C	62.34	62.12	63.05	63.15
%H	4.88	4.67	4.94	4.90
%N	4.85	4.80	4.90	4.92
%O	16.61	16.45	16.80	16.88
%Zn	11.32	11.96	–	–
%Co	–	–	10.31	10.15

Table 1 (Abdelghany et al., 2021; Katouah, 2021). Fig. 1 represents the FT-IR spectra of the Zn(II) and Co(II) complexes, respectively. The bands, which were observed in the Zn(II) and Co(II) complexes at 480 and 430 cm⁻¹, are due to the stretching vibration of Zn-O and Co-O, respectively (Abdelghany et al., 2021; Katouah, 2021; Nakamoto, 2008). The bands, which were observed in the Zn(II) and Co(II) complexes at 582 and 570 cm⁻¹, are due to the stretching vibration of Zn-N and Co-N, respectively. The bands, which were observed in the Zn(II) and Co(II) complexes in the range 690–960 cm⁻¹ and 680–950 cm⁻¹, are due to CH out of plane bend-

ing vibration of aromatic rings, respectively. The bands, which were observed in the Zn(II) and Co(II) complexes at 1390 and 1385 cm⁻¹, are due to the symmetric stretching vibration of COO, respectively. The bands, which were observed in the Zn(II) and Co(II) complexes in the range 1450–1530 cm⁻¹ and 1460–1540 cm⁻¹, are due to the stretching vibration of C = C aromatic, respectively. The bands, which were observed in the Zn(II) and Co(II) complexes at 1601 and 1610 cm⁻¹, are due to the asymmetric stretching vibration of COO, respectively. The bands, which were observed in the Zn(II) and Co(II) complexes at 1640 and 1645 cm⁻¹, are due to the stretching

**Fig. 1** The FT-IR spectra of the Zn(II) (A) and Co(II) (B) complexes.

vibration of C = N, respectively. The bands, which were observed in the Zn(II) and Co(II) complexes at 2900 and 2950 cm⁻¹, are due to the stretching vibration of CH aliphatic, respectively. The bands, which were observed in the Zn(II) and Co(II) complexes at 3200 and 3300 cm⁻¹, are due to the stretching vibration of CH aromatic, respectively. The bands, which were observed in the Zn(II) and Co(II) complexes at 3450 and 3500 cm⁻¹, are due to the stretching vibration of H-O-H, respectively (Abdelghany et al., 2021; Katouah, 2021; Nakamoto, 2008). Table 2 represents the data of TG and DTA analyses for Zn(II) and Co(II) complexes. There are three decomposition steps. The first exothermic step, which was observed in the temperature range of 30–300 °C, is due to the loss of two coordinated water molecules. The second exothermic step, which was observed in the temperature range of 300–550 °C, is because of the decomposition of the organic moiety. The third step, which was observed in the temperature range of 550–1000 °C, is because of oxidation of metal (Zn or Co) i.e., formation of ZnO or Co₃O₄.

3.2. Characterization of ZnO and Co₃O₄ nanoparticles

The ZnO and Co₃O₄ samples were analyzed using X-ray diffraction (XRD) to check their crystalline phases and structures. The XRD patterns of the ZnO and Co₃O₄ samples are presented in Fig. 2A-B, respectively. In the case of ZnO, the principal reflections observed at the 2θ values of 31.80°, 34.40°, 36.30°, 47.50°, 56.60°, 62.90°, 67.90°, 68.80°, 69.90°, 72.50°, and 78.60° assigned (100), (002), (101), (102), (110), (103), (200), (112), (201), (004), and (202) plains, respectively as clarified from the JCPDS No. 36–1451 (Katouah, 2021). In the case of Co₃O₄, the principal reflections observed at the 2θ values of 36.80°, 38.50°, and 44.80° assigned (311), (222), and (400) plains, respectively as clarified from the JCPDS No. 78–1970 (Katouah, 2021). The average crystallite diameter of the ZnO and Co₃O₄ samples is 39.64 and 30.38 nm, respectively. The FT-IR spectra of the ZnO and Co₃O₄ samples are presented in Fig. 3A-B, respectively. The band, which was appeared in the case of ZnO at 485 cm⁻¹, is because of the stretching vibration of Zn-O. The bands, which were appeared in the case of ZnO at 1615 and 3445 cm⁻¹, are because of the bending and stretching vibration of adsorbed water, respectively (Katouah, 2021). The bands, which were appeared in the case of Co₃O₄ at 530 and 630 cm⁻¹, are because of the stretching vibration of Co(II)-O and Co(III)-O, respectively. The bands, which were appeared in the case of Co₃O₄ at 1620 and 3450 cm⁻¹, are because of the bending and stretching vibration of adsorbed water, respectively (Katouah, 2021). The morphology of the ZnO

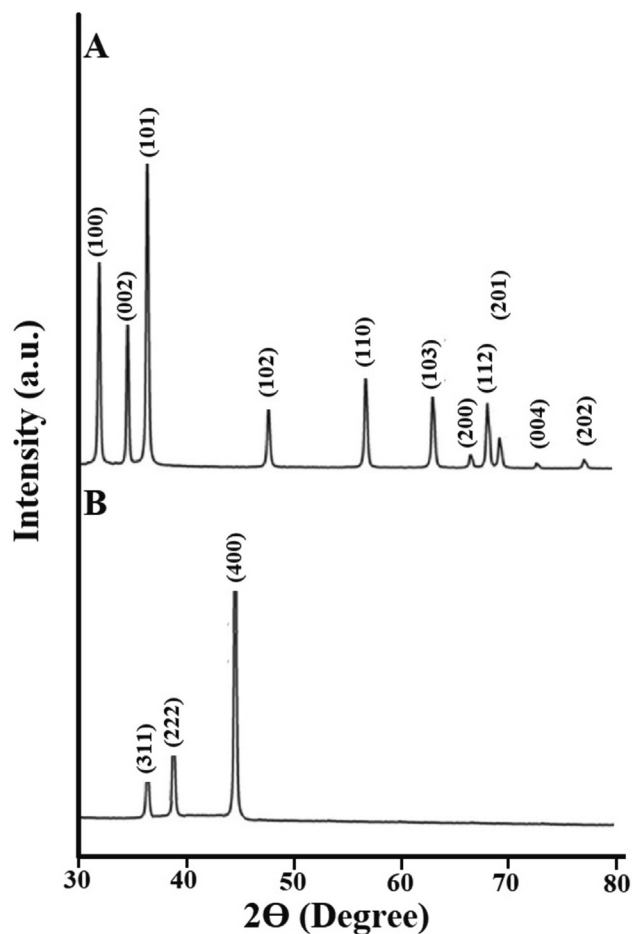


Fig. 2 The XRD patterns of the ZnO (A) and Co₃O₄ (B) samples.

and Co₃O₄ samples was examined via HR-TEM as shown in Fig. 4A-B, respectively. The ZnO and Co₃O₄ samples consist of irregular and spherical shapes with an average diameter of 35.04 and 26.48 nm, respectively. UV-Vis spectrophotometer was utilized for determining the bandgap via the Tauc plot method (Eq. (3)) for the ZnO and Co₃O₄ samples as shown in Fig. 5A-B, respectively (Katouah, 2021).

$$(\rho h\nu)^M = G(h\nu - E_g) \quad (3)$$

where G, ρ, M are a constant, the absorption coefficient, and an integer depending on the type of transition. In the case of a direct allowed transition M equals 2. Besides, in the case of an

Table 2 Thermal analysis of the synthesized complexes.

Steps	Zn(II) complex (C ₃₀ H ₂₈ N ₂ O ₆ Zn)			Co(II) complex (C ₃₀ H ₂₈ N ₂ O ₆ Co)		
	Chemical equations	Weight loss%		Chemical equations	Weight loss%	
		Calculated	Found		Calculated	Found
First step	C ₃₀ H ₂₈ N ₂ O ₆ Zn → C ₃₀ H ₂₄ N ₂ O ₄ Zn + 2H ₂ O↑	6.25	6.38	C ₃₀ H ₂₈ N ₂ O ₆ Co → C ₃₀ H ₂₄ N ₂ O ₄ Co + 2H ₂ O↑	6.30	6.15
Second step	C ₃₀ H ₂₄ N ₂ O ₄ Zn → Zn + C ₃₀ H ₂₄ N ₂ O ₄ ↑	82.65	82.26	C ₃₀ H ₂₄ N ₂ O ₄ Co → Co + C ₃₀ H ₂₄ N ₂ O ₄ ↑	83.37	83.49
Third step	Zn + 1/2O ₂ → ZnO	–	–	3Co + 2O ₂ → Co ₃ O ₄	–	–

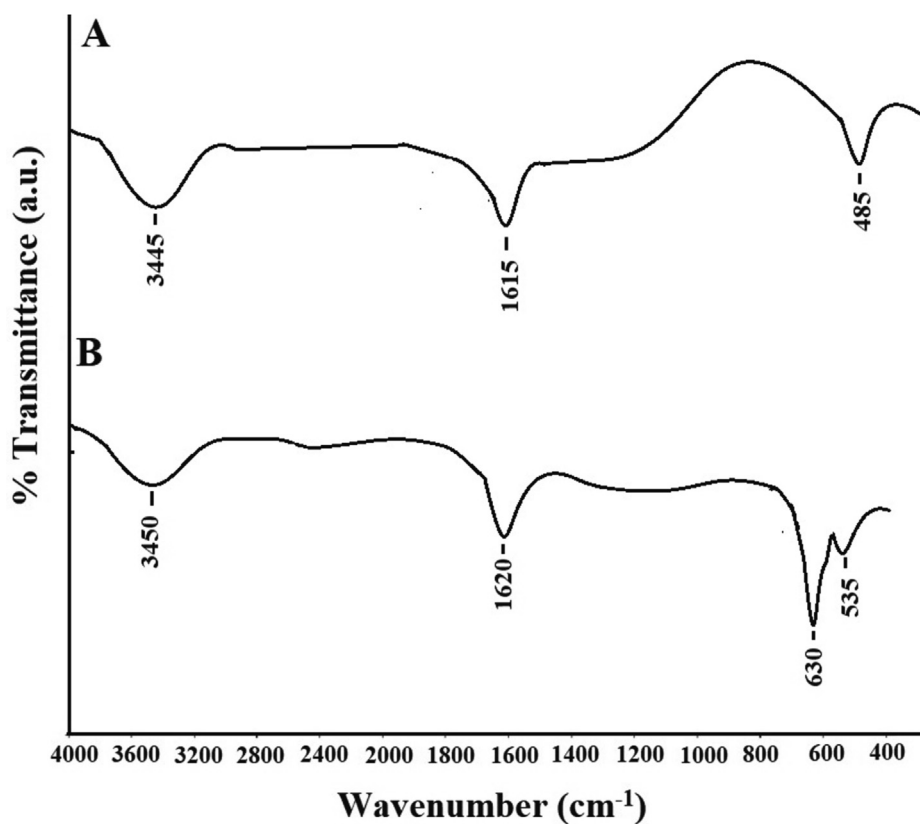


Fig. 3 The FT-IR spectra of the ZnO (A) and Co_3O_4 (B) samples.

indirect allowed transition M equals 0.5. The extrapolating of each graph so as $(\text{ph}\nu)^2$ equals zero gives the optical energy gap (E_g) of the direct allowed transitions. The optical energy gap of the ZnO and Co_3O_4 samples are 2.75 and 3.25 eV, respectively.

3.3. Photocatalytic degradation of methylene blue dye

% A of the methylene blue dye in the dark place using ZnO and Co_3O_4 samples is 8.33 and 18.33 %, respectively. To deter-

mine the influence of UV irradiation time on % D of methylene blue dye using ZnO and Co_3O_4 samples in the absence and presence of H_2O_2 , experiments were performed by the analysis of irradiation time variations versus % D as shown in Fig. 6A-B, respectively. In the absence of hydrogen peroxide, % D increased with increasing UV irradiation time from 20 to 80 min. After that, % D almost remains stable when the UV irradiation time increased from 80 to 120 min owing to the saturation of the active centers. Consequently, the

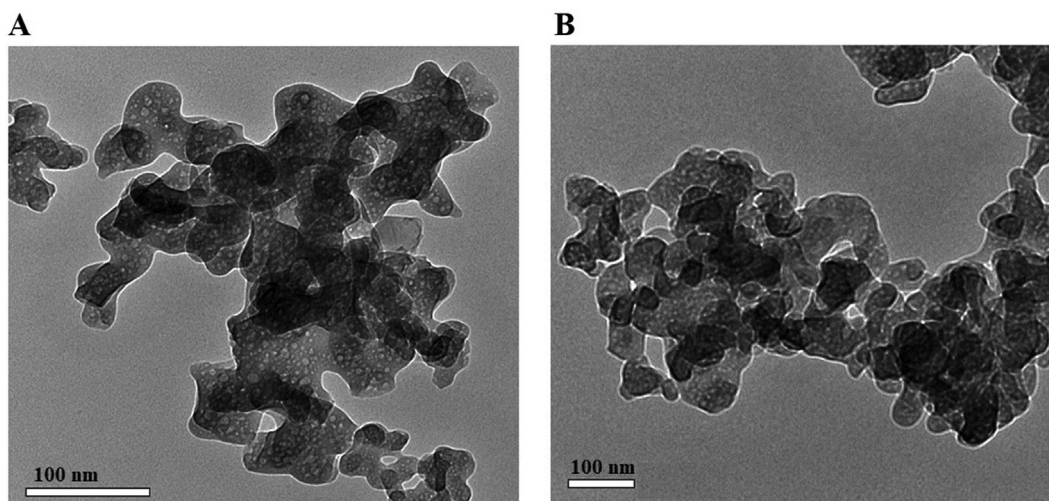


Fig. 4 The HR-TEM images of the ZnO (A) and Co_3O_4 (B) samples.

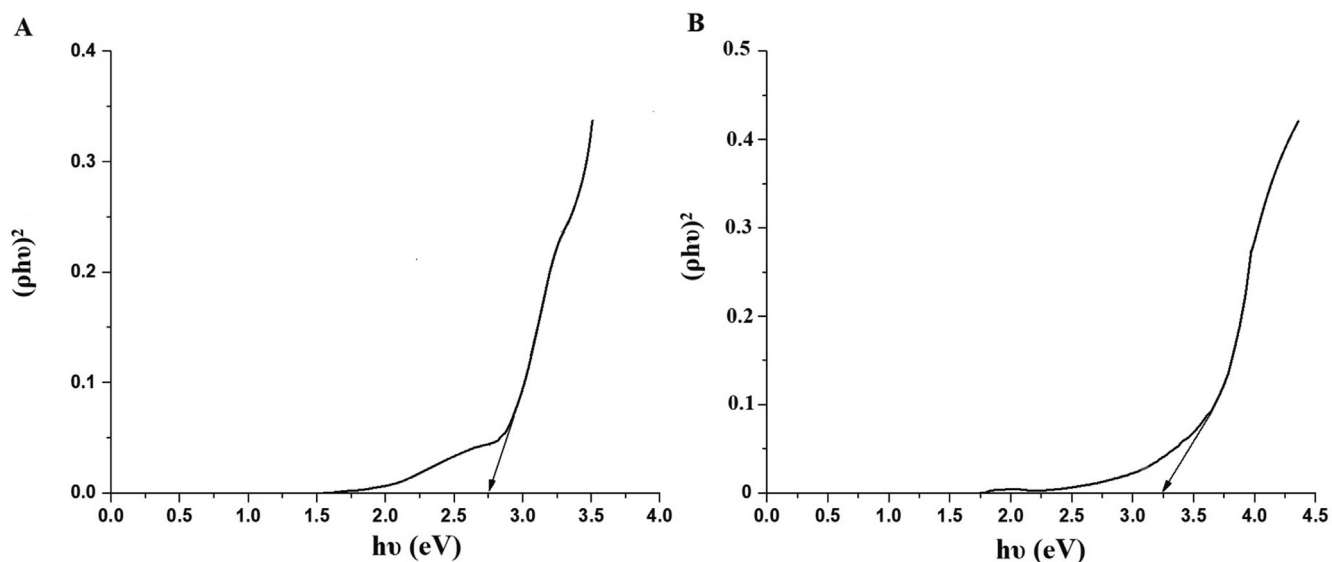


Fig. 5 The optical energy gap of the ZnO (A) and Co₃O₄ (B) samples.

optimum UV irradiation time is 80 min. The % D of the methylene blue dye using ZnO and Co₃O₄ samples after 80 min is 67.27 and 75.51, respectively. In the presence of hydrogen peroxide, % D increased with increasing UV irradiation time from 10 to 40 min. After that, % D almost remains stable when the UV irradiation time increased from 40 to 60 min owing to the saturation of the active centers. Consequently, the optimum UV irradiation time is 40 min. The % D of the methylene blue dye using ZnO and Co₃O₄ samples after 40 min is 94.55 and 98.98, respectively. Photocatalytic degradation of methylene blue dye fitted well with the first-order kinetic model (Eq. (4)) (Katouah, 2021).

$$\ln\left(\frac{Z_2}{Z_3}\right) = Kt \quad (4)$$

where K (1/min) is the first-order constant. The plots of $\ln(Z_2/Z_3)$ versus t in the absence and presence of hydrogen peroxide using ZnO and Co₃O₄ samples are shown in Fig. 7A-B,

respectively. The values of the K and correlation coefficient (R^2) are shown in Table 3. The photocatalytic degradation mechanism of the methylene blue dye can be described as shown in Scheme 2 (Katouah, 2021). Under the impact of UV light irradiation, the ZnO or Co₃O₄ photocatalyst can absorb energy greater than or equals to its energy gap and produce the electron-hole (e^-/h^+) pairs on the surface of ZnO or Co₃O₄. The adsorbed oxygen reacts with electrons to produce oxygen anion radicals. Besides, water molecules react with holes producing hydroxyl radicals. Accordingly, the active kinds produced, especially holes and hydroxyl radicals, react effectively to degrade the methylene blue dye into carbon dioxide, water, or other products. The % D of the methylene blue dye was compared with some catalysts in the literature, for example, Co alloyed CdZnS, ZnWO₄, TiO₂ supported on magnetic core shell, ZnSe, and CdSe as shown in Table 4 (Geetha et al., 2021; de Moura et al., 2021; Sridevi et al., 2020; Ivanets et al., 2021; Ivanets et al., 2019; Ivanets et al., 2021). The

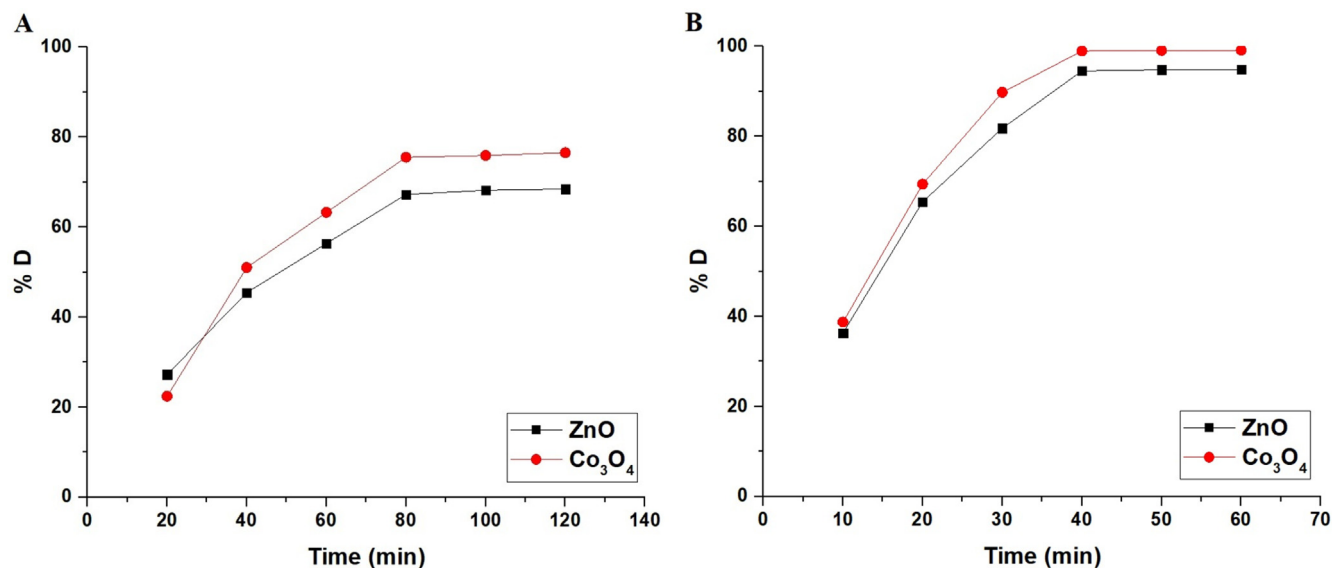


Fig. 6 The plot of % D versus time.

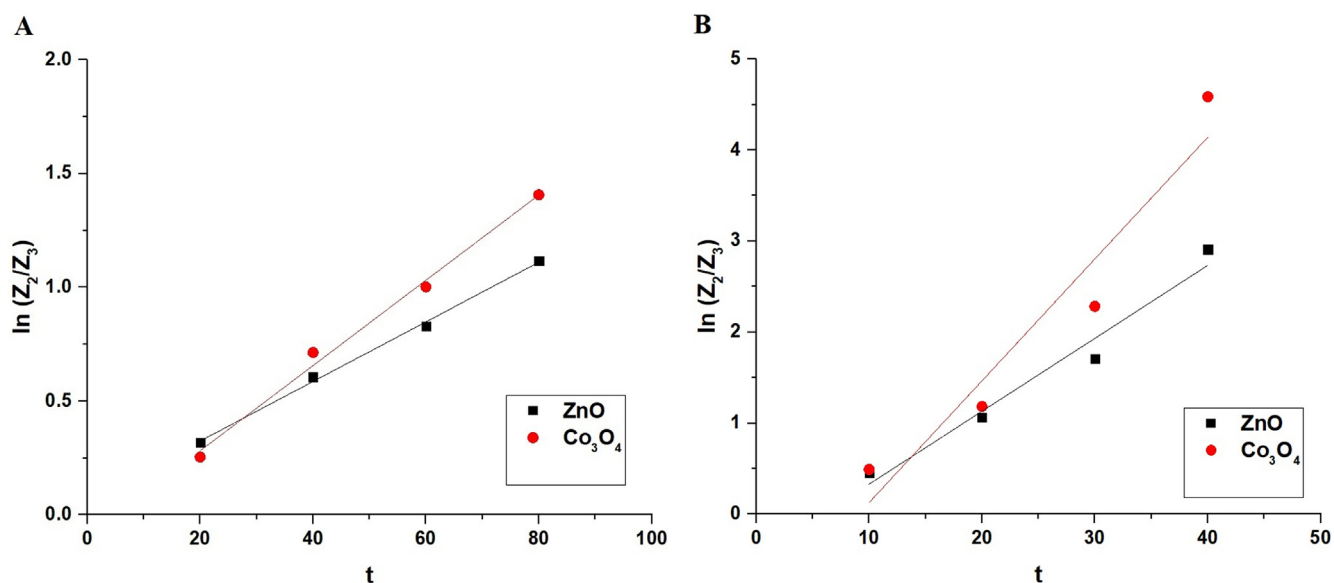
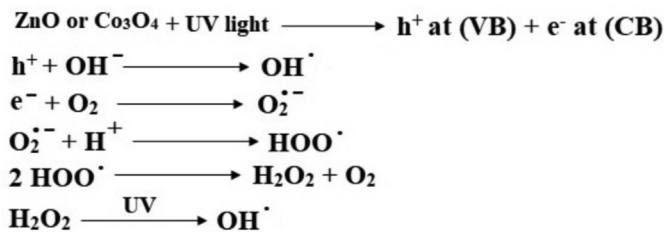
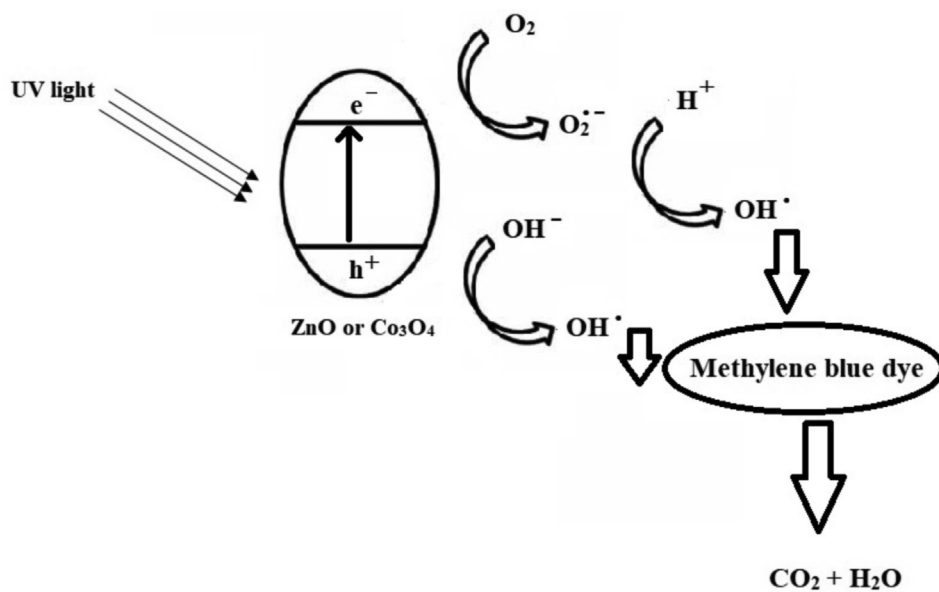


Fig. 7 The plot of $\ln(Z_2/Z_3)$ versus time.

Table 3 Constants of first order model.

Factors	Parameters	
	R^2	K (1/min)
ZnO + UV irradiation	0.986	0.0131
ZnO + UV irradiation + H ₂ O ₂	0.998	0.0801
Co ₃ O ₄ + UV irradiation	0.926	0.0187
Co ₃ O ₄ + UV irradiation + H ₂ O ₂	0.995	0.1338



Scheme 2 The mechanism of the photocatalytic degradation of methylene blue dye.

Table 4 Comparison between % D of methylene blue dye using synthesized nanoparticles and that using different photocatalysts in the literature.

Photocatalyst Name	Dye		E	% Degradation		Ref	
	W (g)	C (mg/L)		V (mL)	Value		Time (min)
Co alloyed CdZnS	0.03	25	25	UV light	83	100	(Geetha et al., 2021)
ZnWO ₄	0.1	10	200	UV light	87	60	(de Moura et al., 2021)
TiO ₂ supported on magnetic core shell	0.03	10	200	UV light	96	120	(Sridevi et al., 2020)
ZnSe	0.05	10	50	UV light	78	150	(Ivanets et al., 2021)
CdSe	0.05	10	50	UV light	56	150	(Ivanets et al., 2021)
ZnO	0.15	60	60	UV light	94.55	40	This study
Co ₃ O ₄	0.15	60	60	UV light	98.98	40	This study

E = Excitation source, V = Volume, C = Concentration, and W = Weight.

Table 5 Biological activity of the synthesized samples.

Sample	Inhibition zone diameter (mm/mg sample)					
	Staphylococcus aureus	Escherichia coli	Pseudomonas aeruginosa	Streptococcus species	Aspergillus species	Candida species
Control	15	13	12	9	12	11
Zn(II) complex	22	21	17	19	17	14
Co(II) complex	19	15	15	16	14	12
ZnO	12	8	8	11	0	0
Co ₃ O ₄	11	10	9	10	0	0

results confirmed the superiority of the ZnO and Co₃O₄ samples for their degrading a high concentration of the methylene blue dye in a shorter time.

3.4. Biological activity

In vitro antimicrobial activities of the metal complexes and their nanoparticles were examined against six microbes using the modified disc diffusion procedure (Katouah, 2021). The zone of inhibition versus the growth of microbes for the metal complexes and their nanoparticles is given in Table 5. The complexes and their nanoparticles diffused into microbes through the lipid layer of spore membranes to the site of action eventually killing them via combining with –OH groups of specific cell enzymes (Katouah, 2021). The diversity in the efficiency of different biocidal agents against different organisms relies on the impermeability of the cell. It is clear that Zn(II) and Co(II) complexes display inhibition towards all the studied microbes. Besides, ZnO and Co₃O₄ nanoparticles exhibit less inhibition towards Staphylococcus aureus, Escherichia coli, Pseudomonas aeruginosa, and Streptococcus species. Moreover, ZnO and Co₃O₄ nanoparticles have no activity towards Aspergillus and Candida species.

4. Conclusions

ZnO and Co₃O₄ nanoparticles were facilely synthesized using the thermal decomposition of novel Zn(II) and Co(II) Schiff base complexes. The average crystallite diameter of the ZnO and Co₃O₄ samples is 39.64 and 30.38 nm, respectively. The % degradation of the methylene blue dye in the presence of hydrogen peroxide using ZnO and Co₃O₄

samples after 40 min is 94.55 and 98.98, respectively. Compared to Schiff base complexes, ZnO and Co₃O₄ nanoparticles exhibit less inhibition towards Staphylococcus aureus, Escherichia coli, Pseudomonas aeruginosa, and Streptococcus species. Moreover, ZnO and Co₃O₄ nanoparticles have no activity towards Aspergillus and Candida species.

Declaration of Competing Interest

The authors declare that they have no known competing financial interests or personal relationships that could have appeared to influence the work reported in this paper.

Acknowledgments

This work was funded by the Deanship of Scientific Research at Princess Nourah Bint Abdulrahman University, through the Research Groups Program Grant No. (RGP-1440-0003) (3).

References

- Abdelghany, M.M., Ahmed, I.S., Dessouki, H.A., Abdelrahman, E.A., 2021. Facile Synthesis of CuO and Ag Nanoparticles by Thermal Decomposition of Novel Schiff Base Complexes. *J. Inorg. Organomet. Polym. Mater.* <https://doi.org/10.1007/s10904-021-02032-y>.
- Abdelrahman, E.A., 2018. Synthesis of zeolite nanostructures from waste aluminum cans for efficient removal of malachite green dye from aqueous media. *J. Mol. Liq.* 253, 72–82.
- Abdelrahman, E.A., Abou El-Reash, Y.G., Youssef, H.M., Kotp, Y.H., Hegazy, R.M., 2021. Utilization of rice husk and waste

- aluminum cans for the synthesis of some nanosized zeolite, zeolite/zeolite, and geopolymer/zeolite products for the efficient removal of Co(II), Cu(II), and Zn(II) ions from aqueous media. *J. Hazard. Mater.* 401, 123813.
- Abdelrahman, E.A., Hegazey, R.M., 2019. Facile Synthesis of HgO Nanoparticles Using Hydrothermal Method for Efficient Photocatalytic Degradation of Crystal Violet Dye Under UV and Sunlight Irradiation. *J. Inorg. Organomet. Polym. Mater.* 29, 346–358.
- Abdelrahman, E.A., Hegazey, R.M., 2019. Utilization of waste aluminum cans in the fabrication of hydroxysodalite nanoparticles and their chitosan biopolymer composites for the removal of Ni(II) and Pb(II) ions from aqueous solutions: Kinetic, equilibrium, and reusability studies. *Microchem. J.* 145, 18–25.
- Alaghaz, A.N.M.A., Zayed, M.E., Alharbi, S.A., 2015. Synthesis, spectral characterization, molecular modeling and antimicrobial studies of tridentate azo-dye Schiff base metal complexes. *J. Mol. Struct.* 1084, 36–45.
- Almehizia, A.A., Al-Omar, M.A., Naglah, A.M., Bhat, M.A., Al-Shakliah, N.S., 2021. Facile synthesis and characterization of ZnO nanoparticles for studying their biological activities and photocatalytic degradation properties toward methylene blue dye. *Alexandria Eng. J.* <https://doi.org/10.1016/j.aej.2021.06.102>.
- Al-Resayes, S.I., Shakir, M., Shahid, N., Azam, M., Khan, A.U., 2016. Synthesis, spectroscopic characterization and in vitro antimicrobial studies of Schiff base ligand, H2L derived from glyoxalic acid and 1,8-diaminonaphthalene and its Co(II), Ni(II), Cu(II) and Zn(II) complexes. *Arab. J. Chem.* 9, 335–343.
- Baltulionis, G., Blight, M., Robin, A., Charalampopoulos, D., Watson, K.A., 2021. The role of propeptide-mediated autoinhibition and intermolecular chaperone in the maturation of cognate catalytic domain in leucine aminopeptidase. *J. Struct. Biol.* 213, 107741.
- de Moura, S.G., Ramalho, T.C., de Oliveira, L.C.A., Dauzakier, L.C.L., Magalhães, F., 2021. Photocatalytic degradation of methylene blue dye by TiO₂ supported on magnetic core shell (Si@Fe) surface. *J. Iran. Chem. Soc.* <https://doi.org/10.1007/s13738-021-02356-z>.
- Dinesh Karthik, A., Shakila, D., Geetha, K., Muthuvel, I., 2020. Green approach to synthesize, spectral investigation and biological applications of potentially active ternary Schiff base copper(II) complexes. *Mater. Today Proc.* 43, 2389–2396.
- Dong, X., Li, Y., Li, Z., Cui, Y., Zhu, H., 2012. Synthesis, structures and urease inhibition studies of copper(II) and nickel(II) complexes with bidentate N, O-donor Schiff base ligands. *J. Inorg. Biochem.* 108, 22–29.
- Donmez, S., Arslan, F., Sari, N., Özkan, E.H., Arslan, H., 2017. Glucose biosensor based on immobilization of glucose oxidase on a carbon paste electrode modified with microsphere-attached l-glycine. *Appl. Biochem.* 64, 745–753.
- Geetha, G.V., Sivakumar, R., Sanjeeviraja, C., Ganesh, V., 2021. Photocatalytic degradation of methylene blue dye using ZnWO₄ catalyst prepared by a simple co-precipitation technique. *J. Sol-Gel Sci. Technol.* 97, 572–580.
- Gyimesi-Forrás, K., Leitner, A., Akasaka, K., Lindner, W., 2005. Comparative study on the use of ortho-phthalaldehyde, naphthalene-2,3-dicarboxaldehyde and anthracene-2,3-dicarboxaldehyde reagents for α -amino acids followed by the enantiomer separation of the formed isoindolin-1-one derivatives using quinine-type chiral stationary phases. *J. Chromatogr. A.* 1083, 80–88.
- Hegazey, R.M., Abdelrahman, E.A., Kotp, Y.H., Hameed, A.M., Subaihi, A., 2020. Facile fabrication of hematite nanoparticles from Egyptian insecticide cans for efficient photocatalytic degradation of rhodamine B dye. *J. Mater. Res. Technol.* 9, 1652–1661.
- Ivanets, A., Roshchina, M., Srivastava, V., Prozorovich, V., Dontsova, T., Nahirniak, S., Pankov, V., Hosseini-Bandegharai, A., Nguyen Tran, H., Sillanpää, M., 2019. Effect of metal ions adsorption on the efficiency of methylene blue degradation onto MgFe₂O₄ as Fenton-like catalysts. *Colloids Surfaces A Physicochem. Eng. Asp.* 571, 17–26.
- Ivanets, A., Prozorovich, V., Sarkisov, V., Roshchina, M., Grigoraviciute-Puroniene, I., Zarkov, A., Kareiva, A., Masindi, V., Wang, C., Srivastava, V., Sillanpää, M., 2021. Effect of magnesium ferrite doping with lanthanide ions on dark-, visible- and UV-driven methylene blue degradation on heterogeneous Fenton-like catalysts. *Ceram. Int.* 47, 29786–29794.
- Ivanets, A., Prozorovich, V., Roshchina, M., Kouznetsova, T., Budeiko, N., Kulbitskaya, L., Hosseini-Bandegharai, A., Masindi, V., Pankov, V., 2021. A comparative study on the synthesis of magnesium ferrite for the adsorption of metal ions: Insights into the essential role of crystallite size and surface hydroxyl groups. *Chem. Eng. J.* 411, <https://doi.org/10.1016/j.cej.2021.128523>.
- Kaczmarek, M.T., Zabiszak, M., Nowak, M., Jastrzab, R., 2018. Lanthanides: Schiff base complexes, applications in cancer diagnosis, therapy, and antibacterial activity. *Coord. Chem. Rev.* 370, 42–54.
- Karmakar, M., Chattopadhyay, S., 2020. Visible light driven photodegradation of methylene blue with two reduced Schiff base complexes of zinc(II): Exploration of their phosphatase mimicking ability. *Polyhedron.* 184, 114527.
- Katouah, H.A., 2021. Facile synthesis of Co₃O₄ and ZnO nanoparticles by thermal decomposition of novel Co(II) and Zn(II) Schiff base complexes for studying their biological properties and photocatalytic degradation of crystal violet dye. *J. Mol. Struct.* 1241, 130676.
- Kiani, M., Bagherzadeh, M., Kaveh, R., Rabiee, N., Fatahi, Y., Dinarvand, R., Jang, H.W., Shokouhimehr, M., Varma, R.S., 2020. Novel Pt-Ag₃PO₄/CdS/chitosan nanocomposite with enhanced photocatalytic and biological activities. *Nanomaterials.* 10, 1–21.
- Latif, M.A., Tofaz, T., Chaki, B.M., Tariqul Islam, H.M., Hossain, M. S., Kudrat-E-Zahan, M., 2019. Synthesis, Characterization, and Biological Activity of the Schiff Base and Its Ni(II), Cu(II), and Zn(II) Complexes Derived from 4-(Dimethylamino)benzaldehyde and S-Benzylidithiocarbamate. *Russ. J. Gen. Chem.* 89, 1197–1201.
- Liang, J., Sun, D., Yang, Y., Li, M., Li, H., Chen, L., 2021. Discovery of metal-based complexes as promising antimicrobial agents. *Eur. J. Med. Chem.* 224, 113696.
- Moitessier, C., Kital, K., Danjou, P.E., Cazier-Dennin, F., 2020. 4-Methoxy-ortho-phthalaldehyde: a promising derivatizing agent for the fluorimetric evaluation of histamine in seafood. *Talanta Open.* 2, 100014.
- Morrow, J.R., Kolasa, K.A., 1992. Cleavage of DNA by nickel complexes. *Inorganica Chim. Acta.* 195, 245–248.
- Nakamoto, K., 2008. *Infrared and Raman Spectra of Inorganic and Coordination Compounds: Part A: Theory and Applications in Inorganic Chemistry*, sixth ed. <http://dx.doi.org/10.1002/978047045840>.
- Nasri, A., Jaleh, B., Nezafat, Z., Nasrollahzadeh, M., Azizian, S., Jang, H.W., Shokouhimehr, M., 2021. Fabrication of g-C₃N₄/Au nanocomposite using laser ablation and its application as an effective catalyst in the reduction of organic pollutants in water. *Ceram. Int.* 47, 3565–3572.
- Nayebi, B., Rabiee, N., Nayebi, B., Shahedi Asl, M., Ramakrishna, S., Jang, H.W., Varma, R.S., Shokouhimehr, M., 2020. Boron nitride-palladium nanostructured catalyst: efficient reduction of nitrobenzene derivatives in water. *Nano Express.* 1, 030012.
- Nguyen, V.H., Nguyen, B.S., Hu, C., Nguyen, C.C., Nguyen, D.L.T., Dinh, M.T.N., Vo, D.V.N., Trinh, Q.T., Shokouhimehr, M., Hasani, A., Kim, S.Y., Van Le, Q., 2020. Novel architecture titanium carbide (Ti₃C₂T_x) mxene cocatalysts toward photocatalytic hydrogen production: A mini-review. *Nanomaterials.* 10, 602–612.
- Nguyen, V.H., Mousavi, M., Ghasemi, J.B., Van Le, Q., Delbari, S.A., Sabahi Namini, A., Shahedi Asl, M., Shokouhimehr, M., Jang, H.

- W., Mohammadi, M., . g-C₃N₄ nanosheet adorned with Ag₃BiO₃ as a perovskite: An effective photocatalyst for efficient visible-light photocatalytic processes. *Mater. Sci. Semicond. Process.* 125, 105651.
- Nguyen, V.H., Mousavi, M., Ghasemi, J.B., Van Le, Q., Delbari, S.A., Shahedi Asl, M., Shokouhimehr, M., Mohammadi, M., Azizian-Kalandaragh, Y., Sabahi Namini, A., 2021b. Insitu preparation of g-C₃N₄ nanosheet/FeOCl: Achievement and promoted photocatalytic nitrogen fixation activity. *J. Colloid Interface Sci.* 587, 538–549.
- Nguyen, V.H., Mousavi, M., Ghasemi, J.B., Van Le, Q., Delbari, S.A., Shahedi Asl, M., Mohammadi, M., Shokouhimehr, M., Sabahi Namini, A., 2021c. High-impressive separation of photoinduced charge carriers on step-scheme ZnO/ZnSnO₃/Carbon dots heterojunction with efficient activity in photocatalytic NH₃ production. *J. Taiwan Inst. Chem. Eng.* 118, 140–151.
- Otani, N., Furuya, T., Katsuomi, N., Haraguchi, T., Akitsu, T., 2021. Synthesis of amino acid derivative Schiff base copper(II) complexes by microwave and wet mechanochemical methods. *J. Indian Chem. Soc.* 98, 100004.
- Saikumari, N., 2021. Synthesis and characterization of amino acid Schiff base and its copper (II) complex and its antimicrobial studies. *Mater. Today Proc.* <https://doi.org/10.1016/j.matpr.2021.02.607>.
- Shokouhimehr, M., Yek, S.M.G., Nasrollahzadeh, M., Kim, A., Varma, R.S., 2019. Palladium nanocatalysts on hydroxyapatite: Green oxidation of alcohols and reduction of nitroarenes in water. *Appl. Sci.* 9, 4183–4193.
- Sridevi, D.V., Ramesh, V., Sundaravadivel, E., 2020. Ultraviolet light induced dye degradation of methylene blue in the presence of photocatalytic CdSe and ZnSe nanoparticles. *Mater. Today Proc.* 42, 1244–1250.
- Srivastava, A.K., Yadav, P., Srivastava, K., Prasad, J., 2021. Synthesis, characterization, biological and electrochemical investigation of copper (II) complexes containing 4-chloro-2-[2, 6-diisopropylphenylimino) methyl] phenol Schiff base ligand and aromatic diinines. *Chem. Data Collect.* 32, 100659.
- Thalamuthu, S., Neelakantan, M.A., 2021. Trinuclear nickel(II) amino acid Schiff base complex containing phenolato and acetato bridges: Structural and functional resemblance of urease. *Inorganica Chim. Acta.* 516, 120109.
- Zhang, K., Hong, K., Suh, J.M., Lee, T.H., Kwon, O., Shokouhimehr, M., Jang, H.W., 2019. Facile synthesis of monodispersed Pd nanocatalysts decorated on graphene oxide for reduction of nitroaromatics in aqueous solution. *Res. Chem. Intermed.* 45, 599–611. <https://doi.org/10.1007/s11164-018-3621-8>.